

Evidence of early deglaciation (18 000 cal a BP) and a postglacial relative sea-level curve from southern Karmøy, south-west Norway

KRISTIAN VASSKOG,^{1,2*}  JOHN-INGE SVENDSEN,¹ JAN MANGERUD,¹ KRISTIAN AGASØSTER HAAGA,¹ ARVE SVEAN¹ and EVA MARIA LUNNAN¹

¹Department of Earth Science and Bjerknes Centre for Climate Research, University of Bergen, Bergen, Norway

²Department of Geography, University of Bergen, Bergen, Norway

Received 18 July 2018; Revised 8 March 2019; Accepted 7 April 2019

ABSTRACT: Based on six consistent radiocarbon dates from the isolation basins Grødheimsvatnet and Kringlemyr, we estimate a minimum deglaciation age for southern Karmøy, an island in outer Boknafjorden (south-west Norway), of around 18 000 calibrated years before present (18k cal a BP). We use microscopic phytoplankton, macrofossils, lithostratigraphic evidence and X-ray fluorescence data to identify the isolation contacts in the basins, and date them to 17.52–17.18k cal a BP in Grødheimsvatnet [15.57 m above present mean sea level (MSL)] and 16.19–15.80k cal a BP in Kringlemyr (11.99 m above MSL). Combining these data with previous studies, we construct a relative sea-level (RSL) curve from 18k cal a BP until the present, which is ~3 ka longer than any previous RSL reconstruction from southern Norway. Following deglaciation, southern Karmøy has experienced a net emergence of around 16–19 m, although with significant RSL fluctuations. This includes two RSL minima well below present MSL around ~13.8 and ~10k cal a BP, and two maxima that culminated around 5–7 m above MSL during the Younger Dryas and early to mid-Holocene, respectively. Considering eustatic sea level and modelled gravitational deformation of the geoid, we estimate a net postglacial isostatic uplift of ~120 m. © 2019 John Wiley & Sons, Ltd

KEYWORDS: Boknafjorden; deglaciation; Karmøy; Scandinavian Ice Sheet; sea level change.

Introduction

There remain large uncertainties in the timing of the last deglaciation of the Scandinavian Ice Sheet (Hughes *et al.*, 2016), and improved ice sheet reconstructions are needed to close the global sea-level budget over the last deglacial period (Clark and Tarasov, 2014). Relative sea-level (RSL) reconstructions from formerly glaciated areas ('near-field' sites) (e.g. Lohne *et al.*, 2007; Long *et al.*, 2011; Shennan *et al.*, 2018), represent an important tool for improving models of Glacial Isostatic adjustment (GIA) (Peltier, 2004; Lecavalier *et al.*, 2014). Integration of empirical data and numerical models will be crucial in future palaeo-ice-sheet reconstructions (Stokes *et al.*, 2015), and the areas that first became deglaciated following the Last Glacial Maximum (LGM) are particularly valuable in this respect, as they can provide the longest available near-field RSL histories (Shennan *et al.*, 2018). Recent studies using cosmogenic exposure dating indicate deglaciation ages of around 20 ka BP for the outer Boknafjorden area in south-west Norway (Svendsen *et al.*, 2015; Gump *et al.*, 2017), making it an ideal location for obtaining long RSL records. However, the cosmogenic exposure age estimates are significantly older than those obtained from radiocarbon dating of adjacent marine records (~18.5k cal a BP) (Sejrup *et al.*, 1994, 2009; Morén *et al.*, 2018), and the timing of deglaciation is therefore poorly constrained in outer Boknafjorden. Most of the fjord was ice-free well before the Younger Dryas (YD) period (Gump *et al.*, 2017), but the marine limits in the inner and middle parts of the fjord are generally younger, coinciding with the culmination of a~10-m transgression in the YD (Helle *et al.*, 2007). In the autumn of 2014, we discovered marine, foraminifera-bearing sediments in the bog Kringlemyr,

located on the island of Karmøy (Fig. 1) at an altitude of about 12 m above present sea level. This is well above the height of the YD transgression predicted by the isobase model of Helle *et al.* (2007), and suggests that the marine limit on southern Karmøy is potentially much older than previously thought. In the present study we therefore address the following main research questions:

- When did the outer part of Boknafjorden become ice-free?
- What is the age and altitude of the marine limit on southern Karmøy?
- How has RSL varied in this area following deglaciation?
- Is it possible to disentangle the different components contributing to the reconstructed near-field RSL signal?

The first question we address through radiocarbon dating of basal sediments from sedimentary sequences on southern Karmøy (Fig. 1). We then use the 'isolation-basin approach' to answer the questions concerning the marine limit and postglacial RSL history. This approach is based on coring basins at different altitudes, before identifying and dating the transition between marine and lacustrine sediments (isolation contacts) or vice versa (ingression contacts). According to Romundset *et al.* (2015) the method was probably first applied by Sundelin (1917), after which it has been widely used in Scandinavia (e.g. Hafsten, 1960; Svendsen and Mangerud, 1987; Lohne *et al.*, 2004, 2007) and other parts of the world (e.g. Shennan *et al.*, 1996; Long *et al.*, 2011; Letham *et al.*, 2016). Isolation- and ingestion contacts are usually recognizable in the sediment as lithostratigraphic boundaries; however, biostratigraphic indicators, such as diatoms (Kjemperud, 1986; Lohne *et al.*, 2007; Letham *et al.*, 2016) or macrofossils (Romundset *et al.*, 2015, 2018), are usually required for a more precise identification of the transitions. Here, we use a combination of lithostratigraphic evidence, macrofossils, geochemistry and microscopic phytoplankton (Kaland, 1984;

*Correspondence: Kristian Vasskog, as above.
E-mail: kristian.vasskog@uib.no

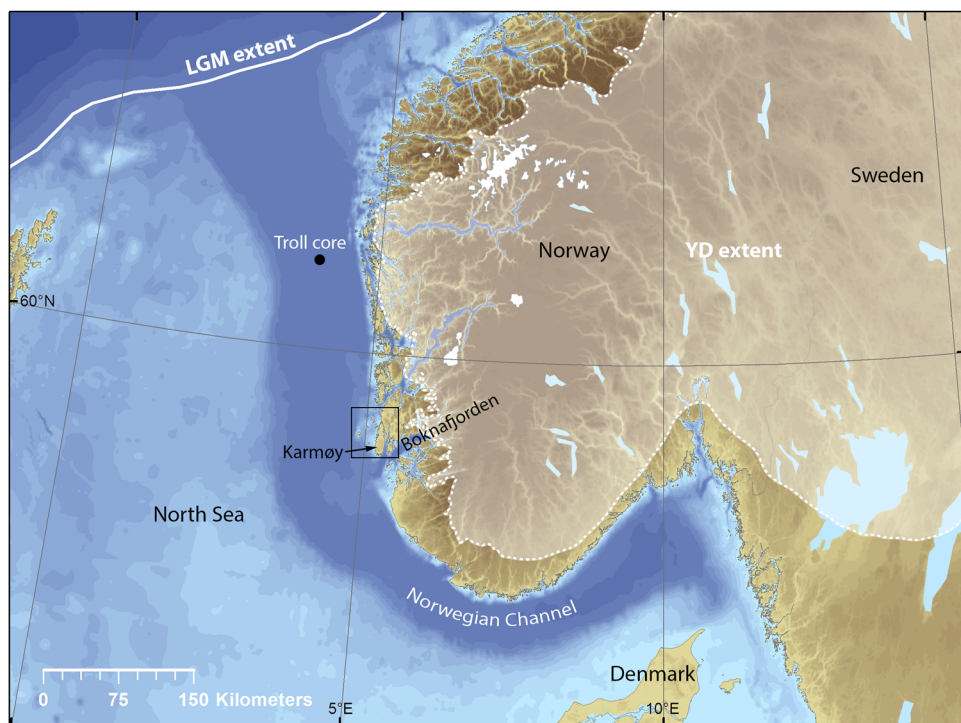


Figure 1. Overview map of southern Norway, showing the location of Karmøy at the mouth of Boknafjorden. The extent of the Scandinavian ice sheet is shown for the Last Glacial Maximum (LGM, white line) and the Younger Dryas (YD, white shading). The LGM extent is from Svendsen *et al.* (2004) and the YD extent is the ‘most credible’ 12 k cal a BP ice margin from Hughes *et al.* (2016). The black box around Karmøy is the area shown in Fig. 2.

Vasskog *et al.*, 2013) to identify isolation contacts in two isolation basins called Grødheimsvatnet (vatnet = lake) and Kringlemyr (myr = bog). This provides two new sea-level index points (SLIPs) for the Lateglacial period on southern Karmøy, which we combine with previous data from several other sites in the outer Boknafjorden region (Anundsen, 1985; Helle *et al.*, 2007; Midtbø, 2011) to construct a complete postglacial RSL curve. The curve is constructed using a statistical procedure that takes into account uncertainties in both age and altitude for the SLIPs and allows us to extract confidence intervals for the reconstruction. In the end we briefly discuss the contribution from different sea-level components to the empirically reconstructed RSL record, namely global eustatic sea level, gravitational deformation of the geoid and isostatic uplift.

Study area

The investigated isolation basins, Grødheimsvatnet and Kringlemyr, are located in the south-west part of Karmøy (Figs. 2, 3), with bedrock outlet thresholds at 15.57 and 11.99 m above mean sea level (MSL), respectively. Grødheimsvatnet has a surface area of 0.12 km² and a drainage area of 0.5 km², whereas the bog surface of Kringlemyr covers 0.02 km², with a surrounding drainage area of 0.1 km². Lacustrine gyttja is found about 2 m below the *Sphagnum*-dominated peaty surface of Kringlemyr, showing that the basin was a freshwater lake before it was infilled and overgrown at some point during the Holocene. The area is dominated by gneissic bedrock (Ragnhildstveit and Solli, 1992), and unconsolidated material is generally sparse in the basin catchments, with the exception of an area immediately north-east of Grødheimsvatnet that features a continuous cover of till (Bergstrøm *et al.*, 2006). Present-day tidal amplitudes are small on southern Karmøy, with a mean high-water spring tide

(MHWST) of 0.22 m and highest astronomical tide (HAT) of 0.45 m above MSL, based on measurements from the nearest (3 km south-east) secondary port Skudeneshavn (Kartverket, 2019). Mean sea level in Skudeneshavn is located 8 cm below the zero level in the Norwegian reference datum NN2000.

Materials and methods

Fieldwork

We measured the altitude of the outlets at the lowest point of the bedrock sills where water currently drains out of the basins, using a GRS-1 differential global positioning system (DGPS) from Topcon Positioning Systems, Inc., equipped with a PG-A1 GPS/Glonass external antenna that enabled real-time kinematic (RTK) measurements with centimetre-scale vertical precision. The outlets were measured to 15.648 ± 0.040 m above MSL for Grødheimsvatnet, and 11.998 ± 0.039 m above MSL for Kringlemyr. Vertical error estimates were calculated as the sum of DGPS instrumental measurement error relative to the EUREF89 ellipsoid, transformation error between the EUREF89 ellipsoid and the NN2000 datum, and error in extrapolation of tidal levels from the nearest standard port (see Supporting Information for details). Both basins have natural bedrock thresholds, and we postulate that no significant erosion has taken place since deglaciation.

A bathymetric survey of Grødheimsvatnet was performed with a Lowrance Elite-5 HDI echo sounder, and a bathymetrical map was produced in the software Reefmaster (Fig. 3). We mapped the sedimentary infill of the lake with a portable EdgeTech 3100-P seismic (chirp) system and visualized the seismic stratigraphy in the free SeiSee software (Fig. 4A). Sediment thickness was estimated from the seismic profiles by applying an acoustic velocity of 1500 m s^{-1} . Two sediment cores were collected from

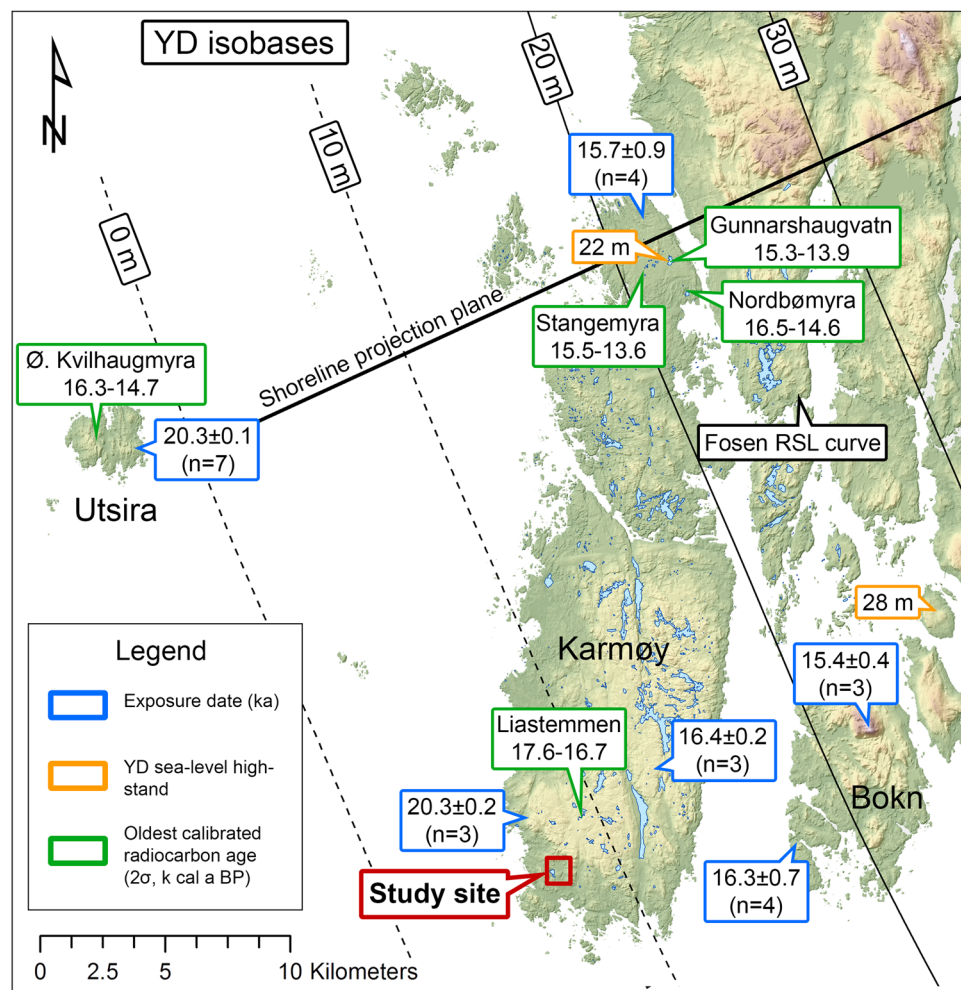


Figure 2. Map showing the islands of Utsira, Karmøy and Bokn (Fig. 1 for location) with isobases for the Younger Dryas (YD) chronozone, adjusted from Helle et al. (2007) (see Supplementary Information for details on the isobase model). Published exposure dates are shown in blue frames as the mean age and standard deviation (in ka) calculated from a given number (*n*) of dates (Svendsen et al., 2015; Gump et al., 2017). Published core sites are shown in green frames, with the oldest radiocarbon date included (2σ k cal a BP). For details, see Paus (1989) (Liastemmen), Paus (1990) (Ø. Kvilstaugmyra) and Helle et al. (2007) (northern Karmøy sites). Altitudes of marine limits dated to the YD are shown in orange, and the reference point used for the Fosen RSL curve in Midtbø (2011) is indicated in black. Our study site on southern Karmøy is marked in red and shown in more detail in Fig. 3.

Grødheimsvatnet in summer 2015, using a raft and 110-mm piston corer able to recover cores up to 5.7 m in length (Nesje, 1992). The 507-04 core (570 cm) filled completely without encountering the dense substratum that makes up the acoustic basement (Fig. 4A). We therefore selected a new coring site in an area with a thinner sedimentary infill about 80 m north-west of the 507-04 site, where the 507-05-core (502 cm long) was retrieved at 11.5-m water depth (Figs. 3,4A). This core penetrated into a diamicton interpreted as basal till, which indicated that we had recovered the base of the postglacial infill.

We cored a transect across Kringlemyr using a 54-mm Russian peat corer in autumn 2014 (Fig. 3), and produced lithostratigraphic logs from each coring point to map the thickness of sedimentary units across the bog (Fig. 4B). No diamicton was recovered in any of the cores, and the corer stopped in bedrock at all sites. Based on the initial mapping we retrieved the 507-01 core, which consists of five half-cylinder, 1-m-long, overlapping sections from 450 to 870 cm depth, from the deepest part of the basin using a 110-mm Russian peat corer. The Kringlemyr master core (507-02) was collected at the same site (Figs. 3,4B) in autumn 2015, using a heavy piston-coring rig able to retrieve 2-m-long contiguous core sections in 110-mm full-cylinder PVC-tubes (constructed by J. Mangerud). We collected the 507-02 master core as three

overlapping sections from two parallel holes, covering a depth from 455 to 883 cm.

Laboratory analyses

The master cores (507-02 and 507-05) were split lengthwise for photography, lithostratigraphical description and further analyses at the EARTHLAB facilities, University of Bergen. Geochemical measurements were performed at 500- μ m intervals in an ITRAX X-ray fluorescence (XRF) core scanner fitted with a molybdenum tube (Croudace et al., 2006), whereas surface magnetic susceptibility was acquired using a Geotek Multi Sensor Core Logger at a down-core resolution of 0.2 cm. We normalized XRF count rates using the sum of coherent and incoherent X-ray scattering to reduce the closed-sum effect and account for changes in organic and water content (Kylander et al., 2011; Davies et al., 2015). After completing the non-destructive analyses, we extracted 1-cm³ samples at 1-cm intervals along the cores and ignited them at 550 °C for 1 h to obtain loss-on-ignition (LOI) as a measure of organic content.

Seven macrofossil samples from Grødheimsvatnet and 11 from Kringlemyr were submitted for accelerator mass spectrometry (AMS) radiocarbon dating at the Poznan Radiocarbon Laboratory in Poland and Beta Analytics, Inc. in Miami, USA

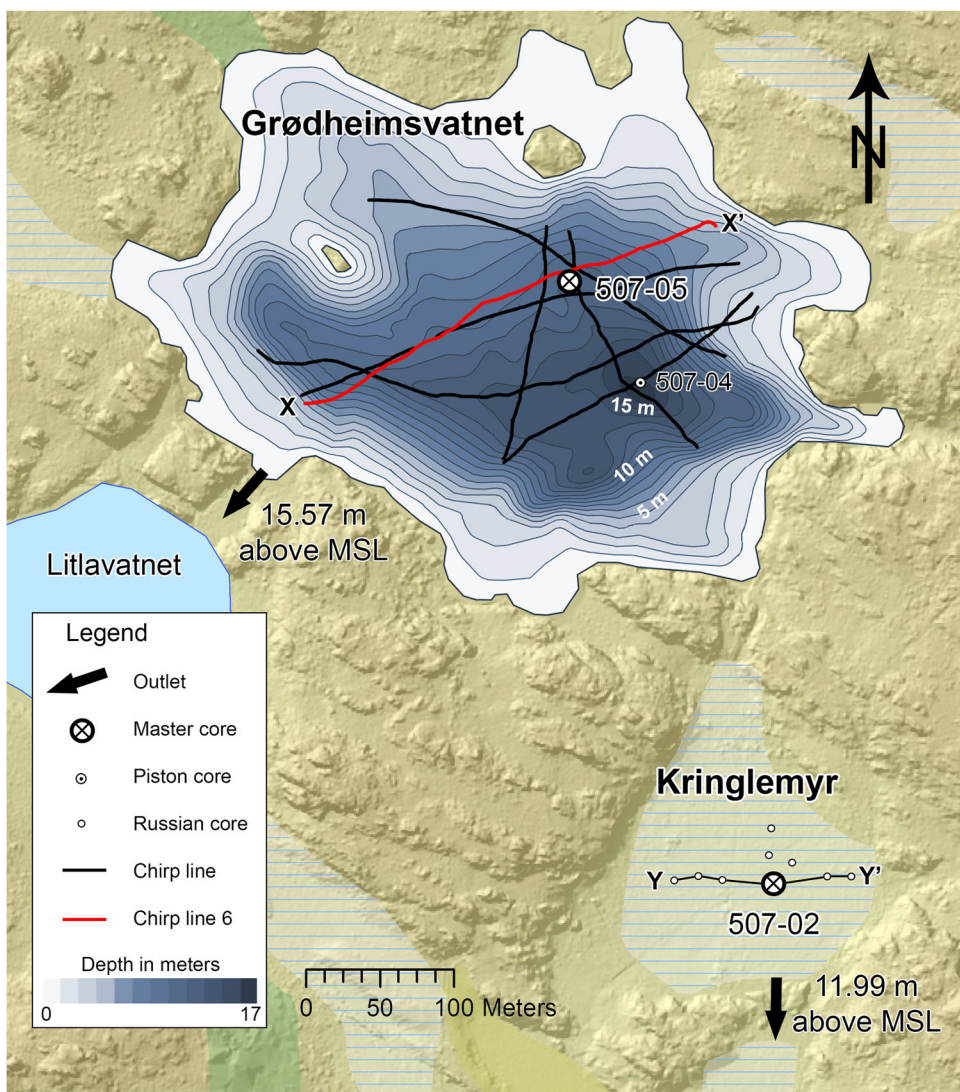


Figure 3. Map of the two investigated basins, Grødheimsvatnet and Kringlemyr, with altitudes of the outlet thresholds shown. Chirp line 6 from Grødheimsvatnet (red line, from X to X') is shown in Fig. 4A, and the core transect across Kringlemyr (Y-Y') is shown in Fig. 4B. Lithostratigraphical logs and selected data from the two master cores 507-05 and 507-02 are shown in Figs. 5, 6, respectively.

(Table 1). Macrofossils were picked under a stereomicroscope after wet sieving 1-cm-thick sediment slices at 125 µm, and in some cases it was necessary to merge adjacent samples to get sufficient material for dating. Terrestrial plant macrofossils, i.e. clearly identifiable leaf fragments, twigs, catkin scales and fruits, were preferred, although aquatic mosses and marine foraminifera were used where terrestrial material was lacking (Table 1). We did not attempt any systematic analysis of foraminiferal species assemblages, but the genus *Elphidium* seemed to dominate our samples. See Figs. 5, 6 for stratigraphical position of all samples screened for foraminifera. The identical stratigraphies of the two parallel cores from Kringlemyr allowed us to transfer the depth of three dated samples from the 507-01 core to the master core based on lithostratigraphic correlation (Table 1). Radiocarbon dates were calibrated in the Clam software (Blaauw, 2010) using the IntCal13 calibration curve for the terrestrial plant remains and aquatic mosses, and the Marine13 curve for the marine material (Reimer *et al.*, 2013). The local ΔR along the Norwegian coast before the Bølling interstadial is unknown, and we therefore used a ΔR of 0 ± 100 years when calibrating the marine dates. Based on the stratigraphical position of a distinct, dark grey layer found at 283 cm depth in core 507-05, we suspected that it could be the Vedde Ash (Mangerud *et al.*,

1984). We extracted a small sediment sample from the layer, and were able to visually identify rhyolitic ash shards under a stereomicroscope. Age-depth models were produced for the cores from Grødheimsvatnet and Kringlemyr using the Clam software (Blaauw, 2010).

Resting cysts of marine-dwelling dinoflagellates (Evitt, 1985) and cell colonies of freshwater-dwelling green algae of the order Chlorococcales (Pentecost, 1984) are commonly observed in palynological studies (Jankovská and Komárek, 2000), and the responses of these two phytoplankton groups are usually sufficient to clearly identify marine-lacustrine transitions in isolation basins (Kaland, 1984). We extracted 1-cm³ samples from 16 and 15 different levels in cores 507-05 and 507-02, respectively, with increased sampling density close to lithostratigraphic boundaries that could potentially represent marine-lacustrine transitions, and submitted them to the standard treatment protocol used to prepare samples for pollen analysis (Fægri and Iversen, 1989). Two tablets of *Lycopodium clavatum* spores (batch 177745, containing $18\ 584 \pm 370$ spores per tablet) were added to each sample before treatment to allow calculation of absolute phytoplankton density and influx (Stockmarr, 1972). The samples were analysed using a Zeiss microscope with $63 \times$ immersion objectives, $12.5 \times$ oculars and phase contrast. A minimum

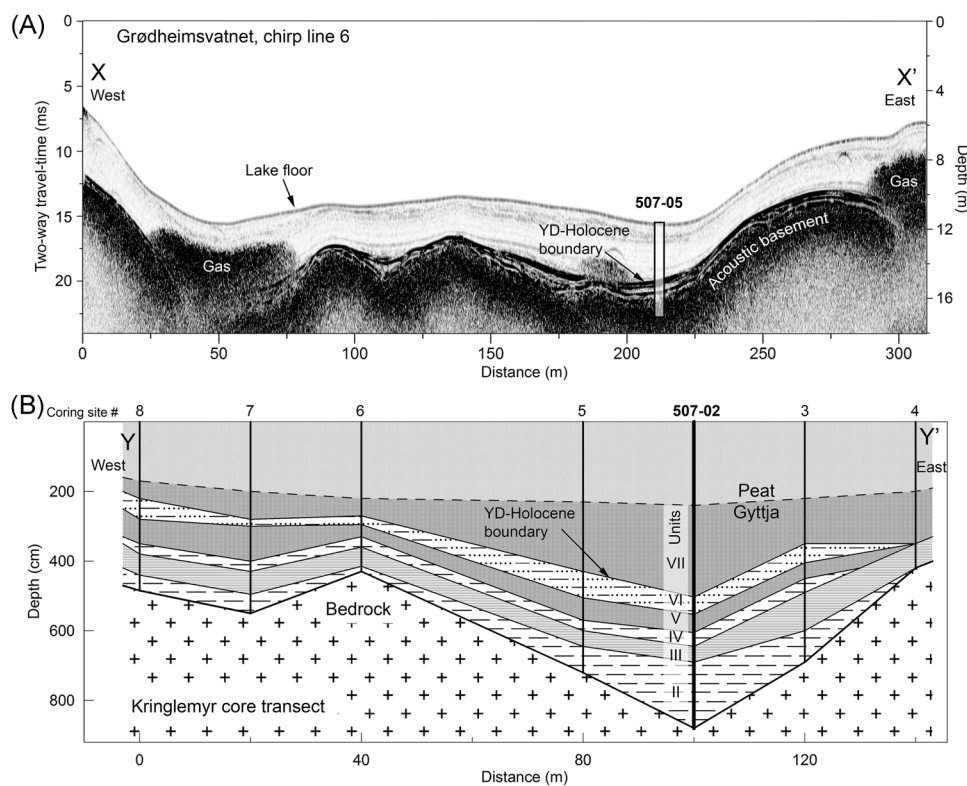


Figure 4. Cross-sections of the sedimentary infill in the two investigated basins. (A) Chirp line 6 from Grødheimsvatnet with location of the 507-05 core indicated. Black 'clouds' are probably gas in the sediment absorbing the seismic signal. The lake floor, YD–Holocene boundary and acoustic basement are indicated. (B) Lithostratigraphic core transect across Kringlemyr with location of the 507-02 master core. See Fig. 3 for locations of transects and Figs. 5,6 for lithostratigraphy, data and interpretations of the master cores.

number of 100 phytoplankton specimens were counted per sample (maximum 613). Specimens of the order Chlorococcales were identified to family or species level using taxonomic keys from Jankovská and Komárek (2000) and Komárek and Jankovská (2001), whereas no further taxonomic classification of dinoflagellate resting cysts was attempted. Knowing that reworked pollen and dinoflagellate cysts are abundant in early Lateglacial sediments from the nearby lake Liastemmen (Paus, 1989), we wanted to investigate the

potential impact of reworked phytoplankton on the results of our analyses. We approached this issue by: (i) analysing samples from the till at the base of core 507-05 to establish which taxa were potentially available for reworking from surrounding till deposits during the Lateglacial, and (ii) registering the total fraction of fragmented phytoplankton specimens in all samples from Grødheimsvatnet. Some brackish-water dinoflagellate species are known to produce resting cysts that can be preserved in palynological samples

Table 1. List of radiocarbon dates from Grødheimsvatnet (core 507-05) and Kringlemyr (cores 507-01 and 507-02).

Core	Lab. code	Depth (cm)	Material	Weight (mg)	¹⁴ C age	Calibrated age (2 σ)	Calibrated age (1 σ)
507-05	Beta-419384	288–289	Terrestrial plant macrofossils	2.8	10 960 ± 50	12 970–12 720	12 860–12 730
507-05	Beta-419385*	293–294	Terrestrial plant macrofossils	2.4	11 240 ± 40	13 180–13 040	13 130–13 070
507-05	LuS-12035	325–330	Insect remains	3.6	12 765 ± 50	15 390–15 040	15 280–15 130
507-05	LuS-12036†	335–340	Insect remains	2.5	12 280 ± 100	14 800–13 930	14 470–14 040
507-05	Beta-419386	397–399	~400 Foraminifera (<i>Elphidium</i> sp.)†	11.6	15 190 ± 50	18 290–17 710	18 140–17 850
507-05	Beta-419387	414–416	~300 Foraminifera (<i>Elphidium</i> sp.)†	14.7	15 270 ± 50	18 370–17 820	18 230–17 950
507-05	Beta-419388	439–441	~200 Foraminifera (<i>Elphidium</i> sp.)†	10.5	15 280 ± 50	18 380–17 830	18 240–17 960
507-02	Poz-73813	503–504	Terrestrial plant macrofossils	10.0	10 140 ± 50	12 040–11 410	11 960–11 647
507-02	Poz-73814	526–527	Terrestrial plant macrofossils	4.7	10 350 ± 60	12 420–11 970	12 380–12 090
507-02	Poz-73815	548–549	Terrestrial plant macrofossils	5.2	11 130 ± 60	13 100–12 820	13 080–12 930
507-01	Beta-386342‡	609–613	Terrestrial plant macrofossils	3.6	12 390 ± 40	14 740–14 170	14 590–14 250
507-01	Beta-386343‡	633–634	Aquatic moss	3.1	13 200 ± 40	16 040–15 700	15 950–15 770
507-02	Beta-439745	637–638	Aquatic moss	9.2	13 260 ± 40	16 100–15 760	16 030–15 850
507-02	Beta-439746	645–647	Terrestrial plant macrofossils	2.9	13 300 ± 50	16 190–15 800	16 090–15 900
507-02	Poz-73816†	767–769	Terrestrial plant macrofossils	23.2	Modern	–	–
507-02	Poz-72817	826–827	Marine algae†	2.8	15 170 ± 80	18 300–17 650	18 140–17 810
507-01	Beta-386344‡	861–866	~300 Foraminifera (<i>Elphidium</i> sp.)†	13.0	15 060 ± 40	18 100–17 560	17 970–17 690
507-02	Poz-73948	876–883	~200 Foraminifera (<i>Elphidium</i> sp.)†	13.6	15 230 ± 80	18 350–17 720	18 210–17 890

*Rejected from the age–depth model.

†Marine dates calibrated using the Marine13 calibration curve with a ΔR of 0 ± 100 years.

‡Depth adjusted from parallel core 507-01 using lithostratigraphic correlation.

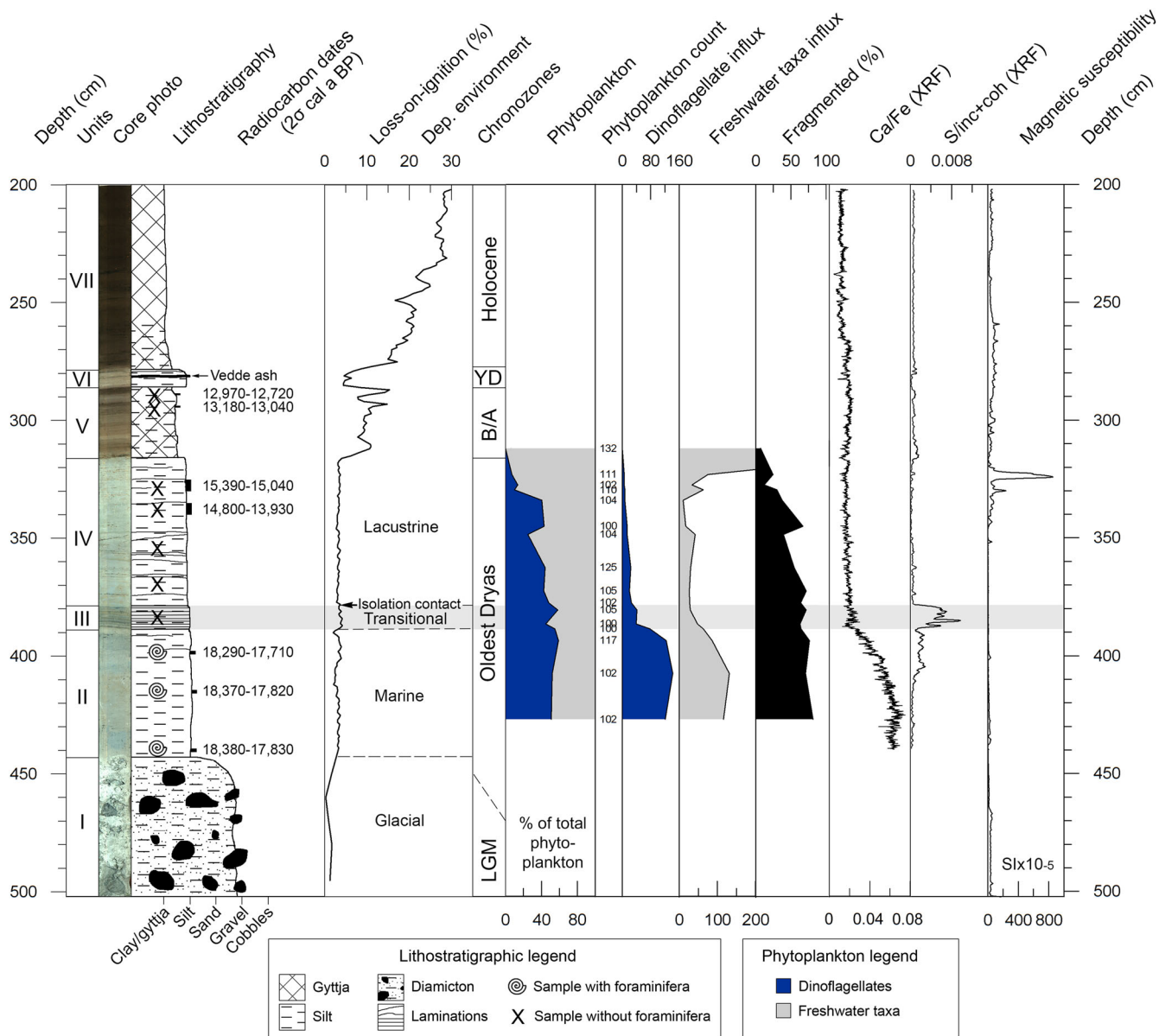


Figure 5. Lithostratigraphy, radiocarbon dates and selected data from core 507-05 from Grødheimsvatnet. Interpreted depositional environments are shown next to the loss-on-ignition curve. Phytoplankton influx (specimens per $\text{cm}^2 \text{a}^{-1}$) was calculated using the age-depth model in Fig. 7A. Chronozone abbreviations: LGM = Last Glacial Maximum; B/A = Bølling–Allerød; YD = Younger Dryas. Magnetic susceptibility is expressed in dimensionless SI units ($\times 10^{-5}$).

(Wall *et al.*, 1973), and some taxa of Chlorococcales can tolerate salinities in the range 3–8‰ (Mur, 1969; Rao *et al.*, 2007; Yoshimura *et al.*, 2013; von Alvensleben *et al.*, 2016). However, for simplicity we refer to dinoflagellate cysts as *marine taxa* and the Chlorococcales as *freshwater taxa* in the main text and figures. Complete phytoplankton abundance and influx diagrams are presented in the Supporting Information, including a suggested preliminary subdivision of the Chlorococcales according to salinity tolerance.

Results

Lithostratigraphy

The chirp survey of Grødheimsvatnet (Fig. 3) revealed an undulating, dense substratum (acoustic basement), which we interpret as bedrock or basal till, covered by an up to ~7-m-thick draping of acoustically layered sediments (Fig. 4A).

The lowermost ~1-m shows high-amplitude seismic reflections, above which the sediments become more acoustically transparent, although still clearly layered. The unconsolidated sediments in Kringlemyr (Fig. 3) have a maximum thickness of about 8.8 m (Fig. 4B), with no observed diamicton at the base. The stratigraphic successions are otherwise very similar in Grødheimsvatnet and Kringlemyr, and we therefore use the same lithostratigraphic subdivision in both basins. Seven distinct units are recognized and numbered from I to VII in depositional order (Figs. 5, 6).

Unit I is only present in Grødheimsvatnet (502–443 cm) and consists of a dense, light-grey diamicton containing angular to subrounded cobbles of up to ~7 cm (longest axis) in a sandy silt/clay matrix (<2% LOI). We interpret this unit as a basal till, indicating that core 507-05 captures the base of the postglacial infill in Grødheimsvatnet.

Unit II is found at 883–691 cm in Kringlemyr and 443–389 cm in Grødheimsvatnet (Figs. 5, 6), and consists of minerogenic, grey silt. In Grødheimsvatnet unit II is mostly

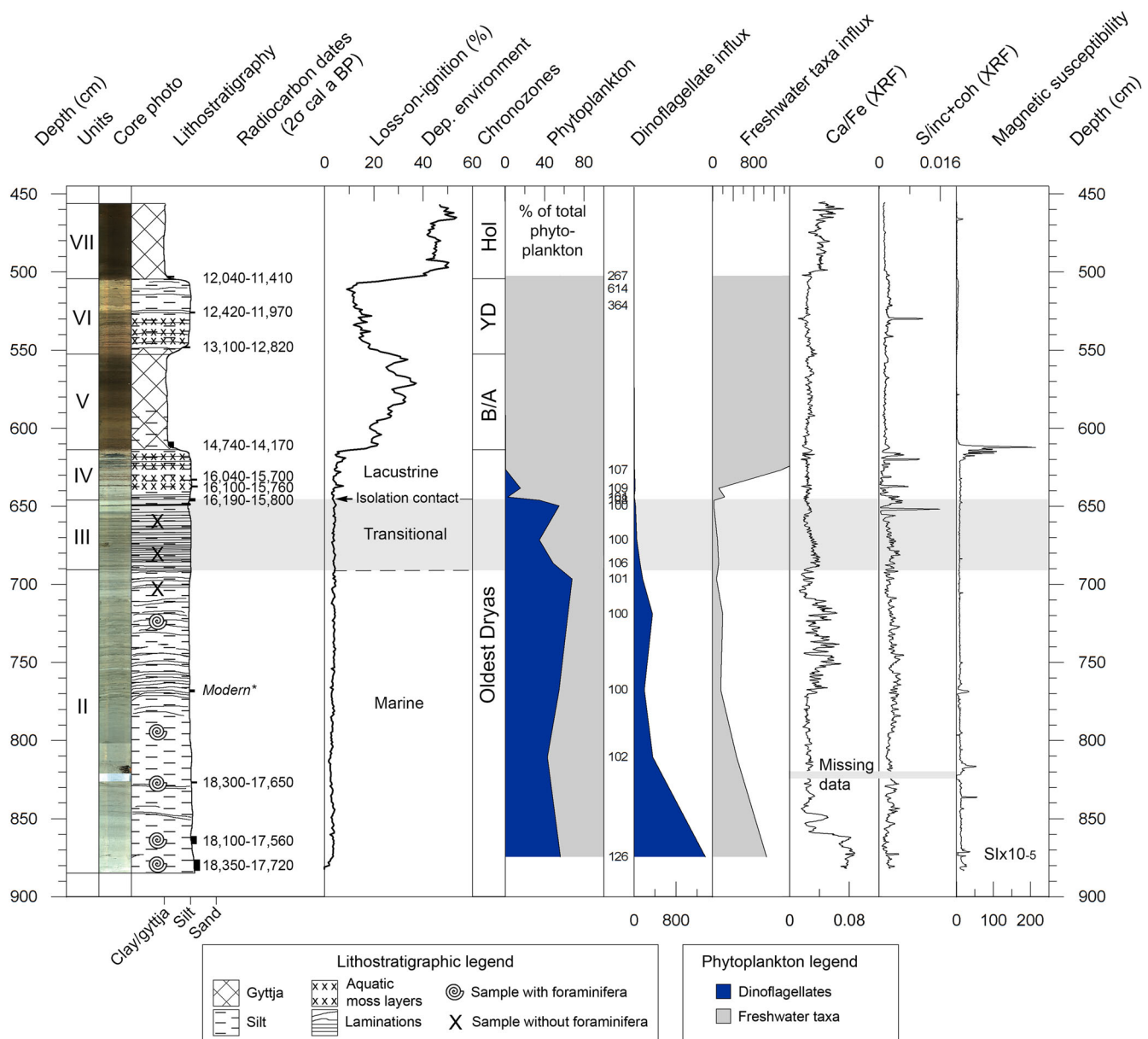


Figure 6. Lithostratigraphy, radiocarbon dates and selected data from core 507-02 from Kringlemyr. Interpreted depositional environments are shown next to the loss-on-ignition curve. Phytoplankton influx (specimens per $\text{cm}^2 \text{a}^{-1}$) was calculated using the age-depth model in Fig. 7B. Chronozone abbreviations: B/A = Bølling–Allerød; YD = Younger Dryas; Hol = Holocene. Magnetic susceptibility is expressed in dimensionless SI units ($\times 10^{-5}$).

massive, with only a few weak laminations towards the top, whereas in Kringlemyr the upper half is laminated throughout, with a zone of slightly stronger laminations from 774 to 755 cm.

Unit III, found at 691–646 cm in Kringlemyr and 389–379 cm in Grødheimsvatnet, has a sharp lower boundary and consists of significantly darker and more strongly laminated silt than that of unit II. In Kringlemyr, the upper part contains a visually distinct 11-cm-thick layer of lighter grey silt with a 1-cm dark layer of sandy silt in the middle.

The overlying unit IV, found between 646 and 614 cm in Kringlemyr and between 379 and 317 cm in Grødheimsvatnet, also consists of mineralogenic silt, but there is a sharp transition to a lighter grey colour and more massive structure compared to unit III. In Kringlemyr, the unit appears laminated, although this is due to layers of aquatic mosses. Contrary to the underlying units, unit IV is thicker in Grødheimsvatnet (62 cm) than in Kringlemyr (32 cm). Overall, units II–IV consist mainly of inorganic silt with LOI below 5%, except for the layers of

aquatic mosses found in unit IV in Kringlemyr, which can be recognized as spikes in the LOI curve.

The lower boundary of unit V reflects a strong increase in organic content, seen as a change from grey to brown colour and an increase in LOI (Figs. 5, 6). In Grødheimsvatnet, the unit is found between 317 and 287 cm, where it consists of light brown, silty gyttja with zones of varying organic content that ranges between 8 and 15% LOI. In Kringlemyr, unit V is found between 614 and 550 cm, consisting of a silty gyttja at the base (~18% LOI) that becomes gradually darker and more organic upwards, and may be classified as gyttja in parts of the upper half (up to 37% LOI).

A new drop in organic content and a change to a lighter, greyish-brown colour marks the lower boundary of unit VI. The transition is relatively rapid in Grødheimsvatnet, where the unit is found between 287 and 279 cm, and more gradual in Kringlemyr, where it is found between 550 and 503 cm. In Kringlemyr LOI decreases gradually upward, with layers of aquatic mosses present in the lower half of the unit.

A relatively rapid transition is seen to the uppermost unit VII, which consists of highly organic, dark brown silty gyttja and pure gyttja. In Kringlemyr, LOI values rise from <10% to >40% within 7 cm of the lower boundary, whereas in Grødheimsvatnet it first rises rapidly from ~5% to >10% before increasing more slowly upward to ~30%. In Kringlemyr there is a gradual transition from lacustrine gyttja to peat around 2 m depth (Fig. 4B).

Chronology

The rhyolitic tephra shards identified in the dark grey layer at 283 cm in core 507-05 are assumed to represent the Vedde Ash (Mangerud *et al.*, 1984), as this is the only known tephra horizon that is commonly observed as a visible layer in western Norwegian Lateglacial sedimentary sequences (e.g. Mangerud *et al.*, 2016). It has been dated to $12\,064 \pm 48$ cal a BP at Kråkenes (Lohne *et al.*, 2014), and this age is added as an additional dating point at 283 cm in the age model for Grødheimsvatnet (Fig. 7). Sample LuS-12036 at 335–340 cm comes out inverted relative to the dates above, and because the sample contains only 0.3 mg C this could easily be due to contamination from younger material. We therefore reject this sample from the age model. Sample Beta-419385 at 293–294 cm produces unrealistically large changes in sedimentation rate if included in the model (Fig. 7A), and this date

is therefore also rejected. We postulate that sedimentation rates have changed gradually through the cores, and apply smooth spline models in Clam (Blaauw, 2010) with the degree of smoothing tuned to the lowest possible value while still avoiding age reversals near the base of the cores. The final smoothing factor is set to 0.5 for Grødheimsvatnet and 0.6 for Kringlemyr (Fig. 7) (default smoothing in Clam is 0.3, whereas a smoothing factor of 1 will produce a linear model similar to a second-order polynomial).

XRF

XRF elements and ratios that have previously been successfully applied as indicators of marine–lacustrine transitions, include the ratio of calcium to iron (Ca/Fe) (Strunk *et al.*, 2018) and sulphur content (Balascio *et al.*, 2011). In Grødheimsvatnet the Ca/Fe ratio shows a very distinct change through the core, with significantly higher ratios in unit II compared to the overlying units and a rapid decrease at the lower boundary of unit III (Fig. 5). A similar pattern is seen in Kringlemyr, although in a zone between 845 and 770 cm in unit II, Ca/Fe values are comparable those seen in the units above (Fig. 6). For sulphur (S/inc + coh), we observe a significant increase in Grødheimsvatnet that is sharply limited to unit III (Fig. 5), whereas no consistent pattern is seen in Kringlemyr (Fig. 6).

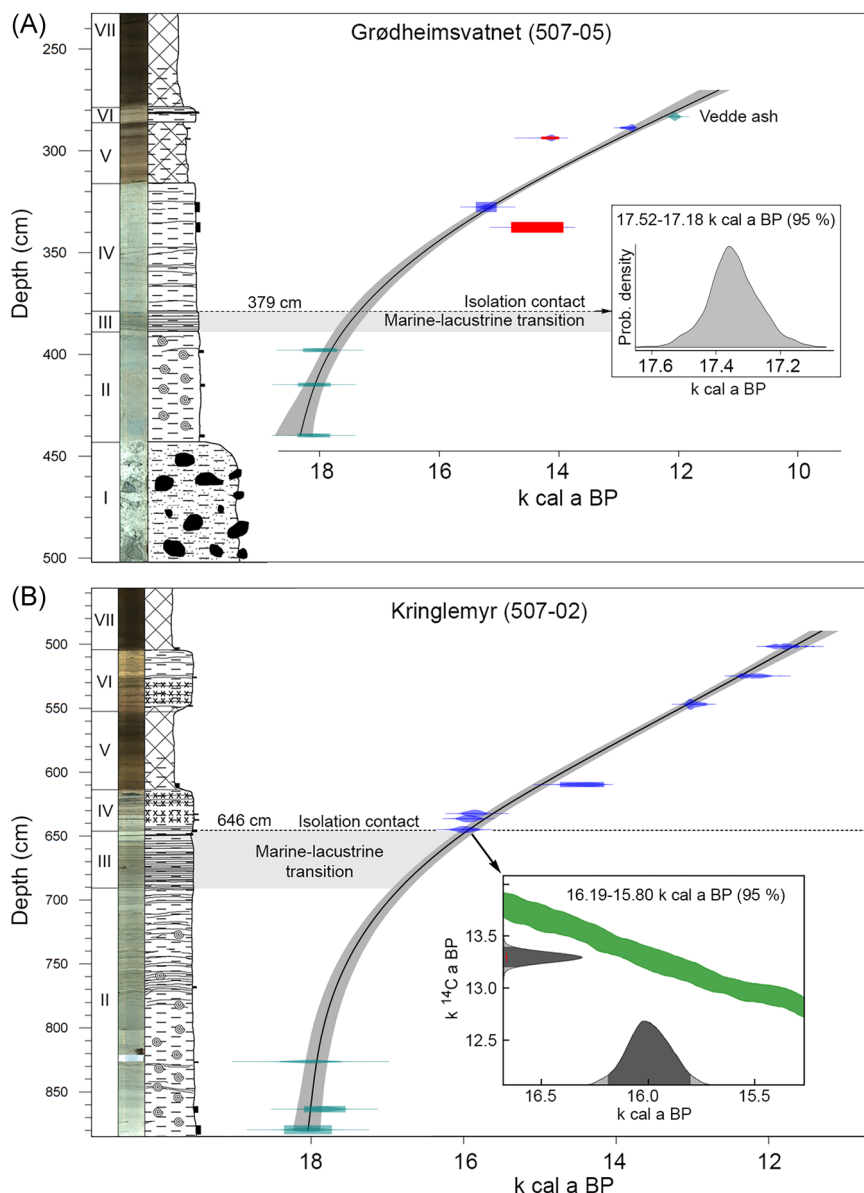


Figure 7. Age–depth models and age estimates for the isolation contacts in Grødheimsvatnet (A) and Kringlemyr (B). See Figs. 5,6 for lithostratigraphic legends. Samples marked red in A are considered outliers. Inset diagrams show the probability distribution for the isolation contact ages, which in A is based on the Clam age–depth model, whereas in B it is obtained directly by calibrating the Beta-439746 sample (645–647 cm, see Table 1) in Clam.

Table 2. Overview of sea-level index points (SLIPs) used in construction of the relative sea-level curve for southern Karmøy (Fig. 8). SLIP01 and SLIP02 are from this study. SLIP03–SLIP08 are from Helle *et al.* (2007) and SLIP09–SLIP15 from Midtbø (2011).

Sea level index point	Site	Original altitude (m)	Distance (km)	Shoreline gradient (m km^{-1})	Mean adjusted altitude (m)	Extrapolation error	Altitude measurement error	Total vertical error (\pm)	Mean age (k cal a BP)	Age uncertainty (ka. 2σ)
SLIP01	Grødheimsvatnet	15.568	–	–	15.228	–	0.04	0.244	17.35	0.17
SLIP02	Kringlemyr	11.909	–	–	11.569	–	0.039	0.243	16	0.2
SLIP03	Nordbømyra	14.98	13.8	1.066 ± 0.09	0.27	1.30	0.50	1.39	15.51	0.95
SLIP04	Storavatnet	19.9	22.3	1.066 ± 0.09	-3.87	2.10	0.50	2.16	13.81	0.36
SLIP05	Nordbømyra	14.98	13.8	1.066 ± 0.09	0.27	1.30	0.50	1.39	12.88	0.34
SLIP06	Gunnarshaugvatn	21.18	13.8	1.066 ± 0.034	6.47	0.47	0.50	0.69	12.35	0.37
SLIP07	Gunnarshaugvatn	21.18	13.8	1.066 ± 0.034	6.47	0.47	0.50	0.69	11.91	0.64
SLIP08	Nordbømyra	14.98	13.8	0.8 ± 0.12	3.94	1.66	0.50	1.73	11.19	0.51
SLIP09	Rabbavatnet	11.3	17.2	0.73 ± 0.11	-1.26	1.88	0.50	1.95	10.93	0.21
SLIP10	Molltjørna	6.5	19	0.55 ± 0.083	-3.95	1.57	0.50	1.65	10.15	0.22
SLIP11	Molltjørna	6.5	19	0.41 ± 0.06	-1.29	1.17	0.50	1.27	9.32	0.17
SLIP12	Røyksund outcrop	9.4	16.1	0.26 ± 0.039	5.21	0.63	0.50	0.80	8.08	0.56
SLIP13	Røyksund outcrop	9.3	16.1	0.16 ± 0.024	6.72	0.39	0.50	0.63	6.66	0.33
SLIP14	Molltjørna	6.5	20	0.06 ± 0.009	5.30	0.18	0.50	0.53	3.91	0.17
SLIP15	Høievatnet	2.8	20.3	0.03 ± 0.0045	2.19	0.09	0.50	0.51	2.25	0.1
SLIP16	Present sea level	–	–	–	0	0	0.1	0.1	-0.068	0.01

Biostratigraphy

In Grødheimsvatnet, foraminifera $>125 \mu\text{m}$ are abundant throughout unit II, before disappearing in unit III (Fig. 5), whereas in Kringlemyr the foraminifera content gradually decreases upwards in unit II, with the uppermost observation at 724 cm depth (Fig. 6). Layers of aquatic mosses are only found in Kringlemyr, where they indicate a lacustrine depositional environment for unit IV (see lithostratigraphic log in Fig. 6).

Altogether 15 microscopic phytoplankton taxa are identified in this study (Supporting Information). The basal till from core 507-05 contains phytoplankton of both marine (38%) and freshwater origin (62%), which is an important observation when considering potential reworking. Most of the freshwater taxa (90%) in the till samples are crumpled or fragmented specimens of *Pediastrum* sp., which also make up a significant part of the phytoplankton found in the cores (10–38%). In Grødheimsvatnet there is a slow and gradual shift from a slight dominance of marine taxa in unit II to a strong dominance of freshwater taxa in the top of unit IV, whereas the absolute influx of all phytoplankton taxa decreases rapidly at the transition between units II and III (Fig. 5). The total percentage of fragmented specimens becomes gradually smaller from the base of the core (81%) and upwards to unit V (6%). In Kringlemyr, there is an abrupt transition from less than 50% to more than 90% freshwater taxa across the boundary between units III and IV (Fig. 6), and the influx of dinoflagellate cysts is reduced from ~ 160 to < 10 specimens $\text{cm}^{-2} \text{ a}^{-1}$ through unit III (Fig. 6).

Discussion

Interpretation of depositional environments

The presence of foraminifera indicates that both basins were fully marine during deposition of unit II (Figs. 5, 6). In Kringlemyr, aquatic mosses in unit VI show that a change from marine to lacustrine conditions must occur at or below

the transition from unit III to IV, and the relative phytoplankton abundance responds abruptly at the transition to unit IV by changing from a slight dominance of marine taxa to strong dominance of freshwater taxa. Thus, the biostratigraphical evidence from Kringlemyr is fairly unambiguous, showing that the upper boundary of unit III at 646 cm probably represents an isolation contact (Fig. 6).

In Grødheimsvatnet, the changes in relative phytoplankton abundance are more difficult to interpret, and we need to consider additional lines of evidence to be able to pinpoint the isolation contact. Knowing that Grødheimsvatnet must have been isolated before Kringlemyr (due to the higher outlet altitude), we find that unit III is the most likely candidate for a marine–lacustrine transitional phase in Grødheimsvatnet based on lithostratigraphic criteria and geochemical variations. Decreasing Ca/Fe ratios in the upper part of unit II indicate a gradually smaller influx of marine-sourced Ca as we approach the lower boundary of unit III (Strunk *et al.*, 2018), whereas the distinct dark laminations and increased sulphur values within the unit itself (Fig. 5) are typical features of a marine–lacustrine transitional phase (Kaland, 1984; Kjemperud, 1986; Svendsen and Mangerud, 1987; Lohne *et al.*, 2007; Balascio *et al.*, 2011; Long *et al.*, 2011; Romundset *et al.*, 2018). Based on this, we interpret the distinct drop in influx of both marine and freshwater phytoplankton taxa at the transition to unit III (Fig. 5) to be mainly a result of reduced erosion by marine wave action and currents in the surrounding phytoplankton-bearing till deposits as the isolation phase commenced. However, the high percentage of fragmented specimens through unit IV suggests a continued contribution from reworked phytoplankton after the isolation, i.e. through subaerial erosion, which implies a very low primary productivity in Grødheimsvatnet at the time. Despite this, a subtle increasing trend can be seen in the influx of freshwater taxa and vice versa for the marine taxa throughout unit IV (Fig. 5), and if we exclude all fragmented phytoplankton specimens from the analysis this trend also becomes slightly clearer (Supporting Information). Our age models suggest that the

lithostratigraphic boundary between unit IV and V reflects climatic amelioration at the start of the Bølling interstadial, similar to what is observed in other Lateglacial lacustrine sequences in western Norway (e.g. Paus, 1989; Krüger *et al.*, 2011). We therefore interpret the strong increase in influx of freshwater taxa at the transition to unit V in both Grødheimsvatnet and Kringlemyr to be climatically driven, and not related to the isolation phase. Based on the multiple converging lines of evidence summarized above we conclude that the isolation contact in Grødheimsvatnet probably coincides with the transition between unit III and IV at a depth of 379 cm in core 507-05 (Fig. 5).

Deglaciation of southern Karmøy

Basal radiocarbon dates in the cores from Grødheimsvatnet and Kringlemyr yield near identical ages of 18.38–17.83 and 18.35–17.72 k cal a BP, respectively (Table 1). In both basins these lowermost dates are consistent with a series of overlying dates (Fig. 7), and together they represent a robust minimum age for the deglaciation of southern Karmøy of around 18 k cal a BP. However, local ΔR has varied over time along the Norwegian coast, particularly during periods of changing ocean currents (e.g. Bard *et al.*, 1994; Björck *et al.*, 2003; Eiriksson *et al.*, 2004). At present, local ΔR is small (between -3 ± 22 and 20 ± 30 years) (Mangerud *et al.*, 2006), but during the YD it was around 250–300 years (Bondevik *et al.*, 2006). It therefore seems likely that ΔR values were higher than present when southern Karmøy first became ice-free, and the added ± 100 -year uncertainty in the calibration of our marine dates might be too small to account for this. The oldest available terrestrial radiocarbon date from southern Karmøy yields 17.6–16.7 k cal a BP, and was obtained from the lake Liastemmen (Fig. 2) (Paus, 1989). However, as this sample was extracted 67 cm above the base of the core, it allows for an earlier deglaciation.

Our basal radiocarbon dates can be compared directly with the marine deglacial chronology of the Norwegian Channel, as this is also based mainly on radiocarbon dates of benthic foraminifera (Sejrup *et al.*, 1994, 2009) that were recently calibrated using the Marine13 curve with a ΔR of zero (Morén *et al.*, 2018). According to the marine chronology, the margin of the Norwegian Channel Ice Stream started to retreat from the shelf edge around 19 k cal a BP, while most of the Norwegian Channel was ice-free by 17.6 k cal a BP (Morén *et al.*, 2018). This would place the ice margin close to Karmøy and Utsira by 18.5 cal a BP, which fits well with our results.

As our dates in principle represent a minimum age estimate for deglaciation, they are not in direct conflict with the older ^{10}Be exposure ages presented by Svendsen *et al.* (2015) (Fig. 2). However, a discrepancy of 2000 years (potentially more with a higher ΔR) seems too large to be explained simply by a delayed onset of sedimentation in our basins following deglaciation. It has been shown that the exposure dates from Utsira, and possibly also those obtained close to our study site on Karmøy (Fig. 2), might theoretically carry a significant (up to ~10%) inheritance due to deep production of ^{10}Be by muons (Briner *et al.*, 2016). Our results seem to support this scenario, as a 10% reduction in age would bring the exposure dates from Utsira (20.3 ± 0.1 ka BP) and the oldest ones from Karmøy (20.3 ± 0.2 ka BP) (Gump *et al.*, 2017) directly in line with our radiocarbon dates. However, if the pre-Bølling ΔR values turn out to be large, an even higher inheritance is needed to explain the discrepancy.

New sea-level index points from southern Karmøy

The indicative meaning of an isolation contact will vary depending on basin hydrology, freshwater discharge and the

level of exposure to wind and waves (Kjemperud, 1986; Shennan *et al.*, 2000, 2018). The outlets of Grødheimsvatnet and Kringlemyr are well shielded by the surrounding topography, and based on the phytoplankton content in the surface sediments of Seiatjørna, a comparable lake where the outlet is currently situated 1 ± 1 cm below MHWST (Supporting Information), we infer that the isolation contacts in this study represent the time when the basin outlets were level with MHWST. To relate our SLIPs to MSL, we therefore adjust the measured outlet elevations down by 0.22 ± 0.01 m to account for the current difference between MSL and MHWST on Karmøy (Kartverket, 2019). Modelled palaeotides for time slices at 16 and 18 ka BP (Ward *et al.*, 2016) show that tidal amplitudes might have been about 0.2 m larger in the Boknafjorden region during the isolation phases of our basins, and we account for this by lowering the outlet elevations by another 0.2 ± 0.2 m. The final elevations relative to MSL for our SLIPs are thus 15.228 ± 0.244 m for Grødheimsvatnet (SLIP01) and 11.569 ± 0.243 m for Kringlemyr (SLIP02). Details of how we calculate total vertical errors for the SLIPs are given in the Supporting Information. The age of SLIP01 is obtained from the age-depth model for Grødheimsvatnet, where we get an age estimate of 17.52 ± 17.18 k cal a BP (2σ) for the lake isolation (Fig. 7A). In Kringlemyr, radiocarbon dating of terrestrial plant remains is available directly at the isolation contact (646 cm). This date (Beta-439746) is in good agreement with a series of six overlying dates (Fig. 7B), thereby providing a robust age estimate for SLIP02 of 16.19 ± 15.80 k cal a BP (2σ).

Extrapolation of sea-level index points from inland sites

Following the isolation of Kringlemyr we have no available SLIPs from southern Karmøy, and therefore need to extrapolate data from nearby areas to construct an RSL curve for the remainder of the postglacial period. Between ca. 16 and 11.2 k cal a BP, we use existing SLIPs from northern Karmøy and Kårstø (Anundsen, 1985; Helle *et al.*, 2007), extrapolated to southern Karmøy along a shoreline projection plane perpendicular to the YD isobases (Fig. 2). We use the original YD isobase direction and curvature from Helle *et al.* (2007), although we adjust the distances between them to fit a linear regression model based on YD maximum levels along the northern shore of Boknafjorden (Supporting Information). The same regression model is used to obtain shoreline gradients of 1.066 ± 0.09 m km $^{-1}$ for the pre-YD period and 1.066 ± 0.034 m km $^{-1}$ for the YD period in Boknafjorden. The SLIPs of Holocene age (with the exception of SLIP08, see Table 2) are based on data from the Fosen area (Fig. 2) (Midtbø, 2011). We extrapolate these SLIPs to southern Karmøy using shoreline gradients obtained from an exponential regression model fitted to shoreline data from Hordaland (Kaland, 1984). To account for the uncertainties introduced by using shoreline gradients from this far away (150 km), we add a substantial error margin when using them to extrapolate the SLIPs from Fosen to our field area (Table 2 and Supporting Information).

Postglacial RSL curve for southern Karmøy

We use the statistical package UncertainData.jl (<https://kahaaga.github.io/UncertainData.jl>) created in the Julia programming language to resample our SLIPs in a way that takes into account uncertainty in two dimensions (age and

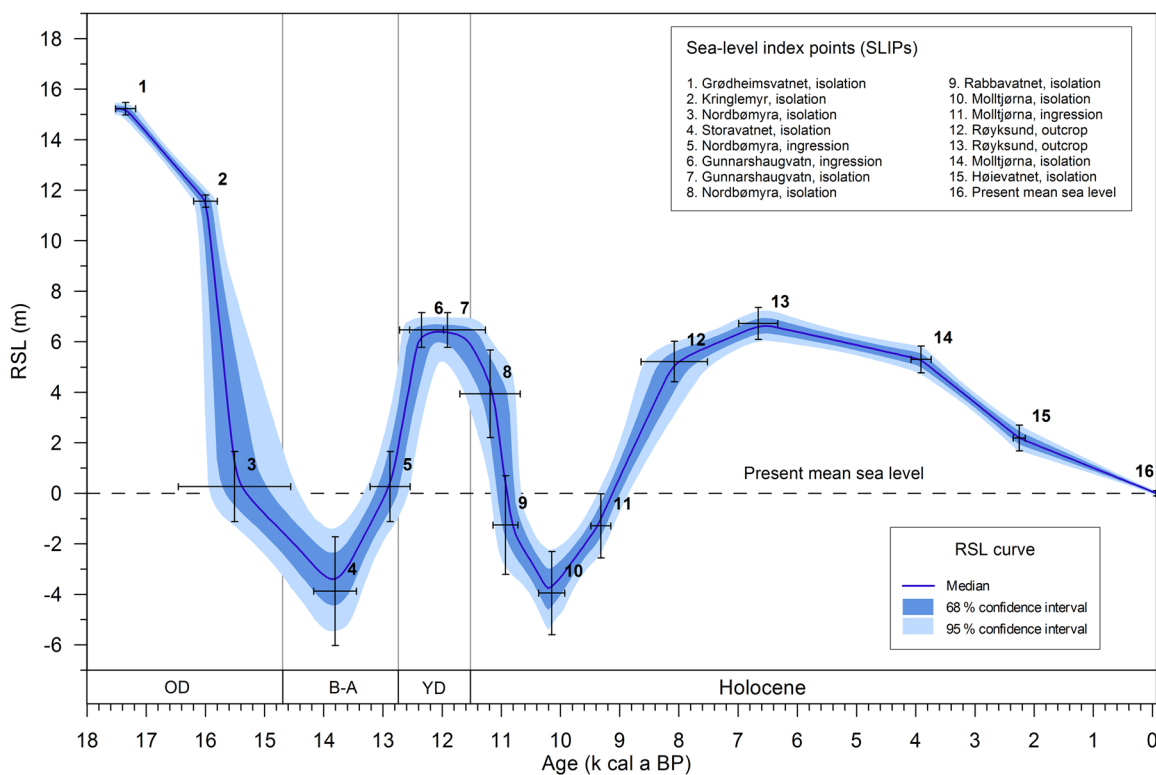


Figure 8. Relative sea-level (RSL) curve for southern Karmøy showing SLIPs with two standard deviation error bars. The median (dark blue), 68% confidence interval (blue) and 95% confidence interval (light blue) are based on 5000 linear interpolations. See Table 2 and Supporting Information for details on SLIPs, error estimates and the statistical procedure used to generate the curve and confidence intervals. Chronozone abbreviations: OD: Oldest Dryas; B-A: Bølling–Allerød; YD: Younger Dryas.

altitude). Vertical uncertainty is set to follow a normal distribution where the SLIP total vertical error (Table 2) defines the two standard deviation range. Age uncertainty uses the complete probability distributions obtained through either calibration of radiocarbon dates or age–depth modelling (Fig. 7; Table 2). For SLIPs where both a radiocarbon- and a pollen-stratigraphical age estimate exist (Helle *et al.*, 2007; Table 2), the calibrated probability distributions are summed and normalized to a single distribution. The final RSL curve (Fig. 8) is constructed by running the resampling procedure 5000 times using linear interpolation and a constraint of strictly decreasing age, meaning that interpolation lines are not allowed to move backwards in time. The most likely (median) curve and associated confidence intervals are then extracted based on the summed two-dimensional probability density of all 5000 interpolation runs (Supporting Information).

Our RSL reconstruction indicates a rate of emergence of about 2.7 m ka^{-1} between the isolations of Grødheimsvatnet and Kringlemyr (SLIP01 and SLIP02, Fig. 8), after which the rate accelerates towards the Bølling–Allerød lowstand. The initial Lateglacial regression phase culminates a few metres below present MSL (Fig. 8), before the RSL trend is reversed sometime before the YD and rises to a maximum of about 5.5–7 m above present MSL in the mid- to late YD. Another phase of rapid regression commences at the transition to the Holocene, reaching a minimum of about 2–5 m below present MSL around 10 k cal a BP. This is followed by the early to mid-Holocene transgression known locally as the Tapes transgression, which culminates 6–7 m above present MSL. From around 7 k cal a BP the curve shows a falling RSL trend towards the present, and a distinct acceleration is seen around 4 k cal a BP, although we have too few data points to properly constrain this knickpoint (Fig. 8). To our knowledge, there are no geomorphological traces of the marine

limit on Karmøy, and we cannot constrain it directly from our RSL curve. A crude extrapolation of our curve back to deglaciation around 18 k cal a BP suggests that it could lie somewhere between 16 and 19 m above present MSL.

Relative sea-level components

Assuming that local changes in steric effects and ocean dynamic topography were small over the postglacial period, subtracting our RSL curve from the eustatic curve of Lambeck *et al.* (2014) should result in a residual signal that includes mainly glacial isostatic uplift (GIA) and gravitational deformation of the geoid (cf. Lohne *et al.*, 2007). We cannot empirically separate these effects, and therefore use results from the global GLAC1-D deglacial ice-sheet chronology (L. Tarasov, pers. comm; Tarasov, 2013; Supporting Information) to estimate the gravitational deformation of the geoid (Fig. 9). By removing this component from the residual signal, we are left with what in theory should represent a ‘clean’ local isostasy signal (green curve in Fig. 9). Based on this approach we estimate a total postglacial uplift of about 120 m for southern Karmøy (Fig. 9). A marked reversal of the reconstructed uplift is seen around 15.3–14.5 k cal a BP (Fig. 9), but this is calculated from a highly uncertain interval in our RSL curve, and we therefore question the validity of this feature. The distinct slowdown in uplift starting in Allerød and continuing through the YD is similar to what Lohne *et al.* (2007) found on Sotra further to the north, and we interpret this as a response to the major re-advance of the Scandinavian Ice Sheet in western Norway during this period (Mangerud *et al.*, 2016). A rapid uplift commences at the start of the Holocene, with a gradual decreasing rate towards the present. The slight acceleration indicated

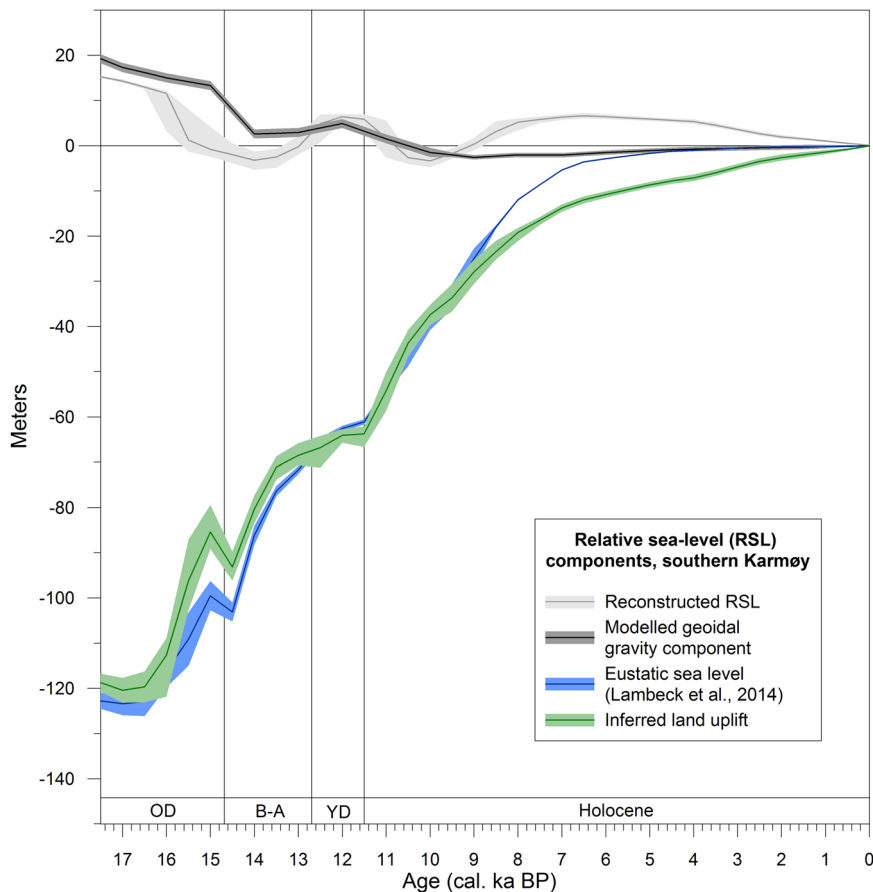


Figure 9. Components of the Karmøy RSL reconstruction (light grey). Inferred land uplift (green) is obtained by subtracting the RSL changes on Karmøy from the global eustatic curve of Lambeck *et al.* (2014) (blue) and adding the modelled gravitational deformation of the geoid (black). All data have been resampled at 0.5-ka intervals (the gravity component was originally modelled in 1-ka time slices, and has therefore been linearly interpolated to 0.5-ka resolution). Uncertainty levels have been propagated to the inferred land uplift by taking the square root of the sum of individual squared uncertainties for the three records used in the calculation. Chronozone abbreviations: OD: Oldest Dryas, B-A: Bølling–Allerød, YD: Younger Dryas.

around 4k cal a BP might not be valid, as we have few SLIPs covering the latter half of the Holocene.

Conclusions

We have studied two isolation basins in the southern part of the island Karmøy, located at the mouth of Boknafjorden in south-west Norway, and conclude that:

- Southern Karmøy became ice-free around 18k cal a BP.
- The isolation basins Grødheimsvatnet (15.65 m above MSL) and Kringlemyr (11.99 m above MSL) became isolated from the sea at 17.52–17.18 and 16.19–15.80k cal a BP, respectively.
- We lack direct evidence of the altitude of the marine limit, but it probably coincides in time with the deglaciation at 18k cal a BP. Extrapolating our RSL curve suggests an altitude range of 16–19 m above present MSL.
- By combining our new data with previous SLIPs available from nearby sites, we construct an RSL curve for southern Karmøy covering the period from 18k cal a BP until present. This is ~3 ka further back in time than any previous RSL reconstruction for southern Norway.
- Correcting for eustatic sea level and gravitational deformation of the geoid suggests a total postglacial isostatic uplift of about 120 m on southern Karmøy.

Supporting information

Additional supporting information can be found in the online version of this article.

File S1. Additional information on uncertainty estimates, construction of the RSL curve, modelled gravitational deformation of the geoid, and phytoplankton analyses.

File S2. RSL curve median and confidence intervals at 50-year resolution.

Acknowledgements. We extend our thanks to Eivind W.N. Støren, Torgeir O. Røthe and Kjetil Bakken, who contributed during fieldwork, and Anne Bjune and Aage Paus, who helped identify plant macrofossils for dating. Lev Tarasov provided modelling results for the gravitational deformation of the geoid, and Anna Hughes provided the map data used in Fig. 1. We are grateful to Rob Barnett and an anonymous reviewer, who provided detailed comments that greatly improved the manuscript. This study is part of the project Eurasian Ice Sheet and Climate Interaction (EISCLIM), funded through the Norwegian Research Council (project No. 229788).

ORCID

Kristian Vasskog  <http://orcid.org/0000-0002-4703-959X>

Abbreviations. AMS, accelerator mass spectrometry; DGPS, differential global positioning system; GIA, glacial isostatic adjustment; HAT, highest astronomical tide; LGM, Last Glacial Maximum; LOI, loss-on-ignition; MHWST, mean high-water spring tide; MSL, mean sea level; RSL, relative sea level; RTK, real-time kinematic; SLIPs, sea level index points; XRF, X-ray fluorescence; YD, Younger Dryas.

References

- Anundsen K. 1985. Changes in shore-level and ice-front position in Late Weichsel and Holocene, southern Norway. *Norsk Geografisk Tidsskrift - Norwegian Journal of Geography* **39**: 204–225. <https://doi.org/10.1080/00291958508552149>
- Balascio NL, Zhang Z, Bradley RS *et al.* 2011. A multi-proxy approach to assessing isolation basin stratigraphy from the Lofoten Islands, Norway. *Quaternary Research* **75**: 288–300. <https://doi.org/10.1016/j.yqres.2010.08.012>
- Bard E, Arnold M, Mangerud J *et al.* 1994. The North Atlantic atmosphere-sea surface ^{14}C gradient during the Younger Dryas

- climatic event. *Earth and Planetary Science Letters* **126**: 275–287. [https://doi.org/10.1016/0012-821X\(94\)90112-0](https://doi.org/10.1016/0012-821X(94)90112-0)
- Bergstrøm B, Olsen L, Riiber K et al. 2006. Rogaland Fylke, *Quaternary Geological Map, 1: 200000*. Norwegian Geological Survey.
- Björck S, Koç N, Skog G. 2003. Consistently large marine reservoir ages in the Norwegian Sea during the Last Deglaciation. *Quaternary Science Reviews* **22**: 429–435. [https://doi.org/10.1016/S0277-3791\(03\)00002-7](https://doi.org/10.1016/S0277-3791(03)00002-7)
- Blaauw M. 2010. Methods and code for ‘classical’ age-modelling of radiocarbon sequences. *Quaternary Geochronology* **5**: 512–518. <https://doi.org/10.1016/j.quageo.2010.01.002>
- Bondevik S, Mangerud J, Birks HH et al. 2006. Changes in North Atlantic radiocarbon reservoir ages during the Allerød and Younger Dryas. *Science* **312**: 1514–1517. <https://doi.org/10.1126/science.1123300>
- Briner JP, Goehring BM, Mangerud J et al. 2016. The deep accumulation of ¹⁰Be at Utsira, southwestern Norway: implications for cosmogenic nuclide exposure dating in peripheral ice sheet landscapes. *Geophysical Research Letters* **43**: 9121–9129. <https://doi.org/10.1002/2016GL070100>
- Clark PU, Tarasov L. 2014. Closing the sea level budget at the Last Glacial Maximum. *Proceedings of the National Academy of Sciences of the United States of America* **111**: 15861–15862. <https://doi.org/10.1073/pnas.1418970111>
- Croudace IW, Rindby A, Rothwell RG. 2006. ITRAX: description and evaluation of a new multi-function X-ray core scanner. *Geological Society, London, Special Publications* **267**: 51–63.
- Davies SJ, Lamb HF, Roberts SJ. 2015. Micro-XRF core scanning in palaeolimnology: recent developments. In *Micro-XRF Studies of Sediment Cores*, Croudace IW, Rothwell RG (eds). Springer: Berlin; 189–226.
- Eiríksson J, Larsen G, Knudsen KL et al. 2004. Marine reservoir age variability and water mass distribution in the Iceland Sea. *Quaternary Science Reviews* **23**: 2247–2268. <https://doi.org/10.1016/j.quascirev.2004.08.002>
- Evitt WR. 1985. Sporopollenin Dinoflagellate Cysts: Their Morphology and Interpretation. American Association of Stratigraphic Palynologists Foundation: Dallas.
- Fægri K, Iversen J. 1989. *Textbook of Pollen Analysis*. Wiley: Chichester.
- Gump DJ, Briner JP, Mangerud J et al. 2017. Deglaciation of Boknafjorden, south-western Norway. *Journal of Quaternary Science* **32**: 80–90. <https://doi.org/10.1002/jqs.2925>
- Hafsten U. 1960. Pollen-analytic Investigations in South Norway: vegetation, climate, shore-line displacement, land occupation. In *Geology of Norway*, Holthedral O (ed). Norwegian Geological Survey, 434–462.
- Helle SK, Rye N, Stabell B et al. 2007. Neotectonic faulting and the Late Weichselian shoreline gradients in SW Norway. *Journal of Geodynamics* **44**: 96–128. <https://doi.org/10.1016/j.jog.2007.01.001>
- Hughes ALC, Gyllencreutz R, Lohne ØS et al. 2016. The last Eurasian ice sheets—a chronological database and time-slice reconstruction, DATED-1. *Boreas* **45**: 1–45. <https://doi.org/10.1111/bor.12142>
- Jankovská V, Komárek J. 2000. Indicative value of Pediastrum and other coccal green algae in palaeoecology. *Folia Geobotanica* **35**: 59–82. <https://doi.org/10.1007/BF02803087>
- Kaland PE. 1984. Holocene shore displacement and shorelines in Hordaland, western Norway. *Boreas* **13**: 203–242. <https://doi.org/10.1111/j.1502-3885.1984.tb00070.x>
- Kartverket. 2019. *Tide Tables for the Norwegian Coast and Svalbard*. The Norwegian Mapping Authority: Stavanger.
- Kjemperud A. 1986. Late Weichselian and Holocene shoreline displacement in the Trondheimsfjord area, central Norway. *Boreas* **15**: 61–82. <https://doi.org/10.1111/j.1502-3885.1986.tb00744.x>
- Komárek J, Jankovská V. 2001. *Review of the green algal genus Pediastrum; implication for Pollen Analytical Research*. J Cramer: Berlin.
- Krüger LC, Paus A, Svendsen JI et al. 2011. Lateglacial vegetation and palaeoenvironment in W Norway, with new pollen data from the Sunnmøre region. *Boreas* **40**: 616–635. <https://doi.org/10.1111/j.1502-3885.2011.00213.x>
- Kylander ME, Ampel L, Wohlfarth B et al. 2011. High-resolution X-ray fluorescence core scanning analysis of les Echets (France) sedimentary sequence: new insights from chemical proxies. *Journal of Quaternary Science* **26**: 109–117. <https://doi.org/10.1002/jqs.1438>
- Lambeck K, Rouby H, Purcell A et al. 2014. Sea level and global ice volumes from the Last Glacial Maximum to the Holocene. *Proceedings of the National Academy of Sciences* **111**: 15296–15303. <https://doi.org/10.1073/pnas.1411762111>
- Lecavalier BS, Milne GA, Simpson MJR et al. 2014. A model of Greenland ice sheet deglaciation constrained by observations of relative sea level and ice extent. *Quaternary Science Reviews* **102**: 54–84. <https://doi.org/10.1016/j.quascirev.2014.07.018>
- Letham B, Martindale A, Macdonald R et al. 2016. Postglacial relative sea-level history of the Prince Rupert area, British Columbia, Canada. *Quaternary Science Reviews* **153**: 156–191. <https://doi.org/10.1016/j.quascirev.2016.10.004>
- Lohne ØS, Bondevik S, Mangerud J et al. 2004. Calendar year age estimates of Allerød–Younger Dryas sea-level oscillations at Os, western Norway. *Journal of Quaternary Science* **19**: 443–464. <https://doi.org/10.1002/jqs.846>
- Lohne ØS, Bondevik S, Mangerud J et al. 2007. Sea-level fluctuations imply that the Younger Dryas ice-sheet expansion in western Norway commenced during the Allerød. *Quaternary Science Reviews* **26**: 2128–2151. <https://doi.org/10.1016/j.quascirev.2007.04.008>
- Lohne ØS, Mangerud J, Birks HH. 2014. IntCal13 calibrated ages of the Vedde and Saksunarvatn ashes and the Younger Dryas boundaries from Kråkenes, western Norway. *Journal of Quaternary Science* **29**: 506–507. <https://doi.org/10.1002/jqs.2722>
- Long AJ, Woodroffe SA, Roberts DH et al. 2011. Isolation basins, sea-level changes and the Holocene history of the Greenland Ice Sheet. *Quaternary Science Reviews* **30**: 3748–3768. <https://doi.org/10.1016/j.quascirev.2011.10.013>
- Mangerud J, Aarseth I, Hughes ALC et al. 2016. A major re-growth of the Scandinavian Ice Sheet in western Norway during Allerød–Younger Dryas. *Quaternary Science Reviews* **132**: 175–205. <https://doi.org/10.1016/j.quascirev.2015.11.013>
- Mangerud J, Bondevik S, Gulliksen S et al. 2006. Marine ¹⁴C reservoir ages for 19th century whales and molluscs from the North Atlantic. *Quaternary Science Reviews* **25**: 3228–3245. <https://doi.org/10.1016/j.quascirev.2006.03.010>
- Mangerud J, Lie SE, Furnes H et al. 1984. A Younger Dryas ash bed in western Norway, and its possible correlations with tephra in cores from the Norwegian Sea and the North Atlantic. *Quaternary Research* **21**: 85–104. [https://doi.org/10.1016/0033-5894\(84\)90092-9](https://doi.org/10.1016/0033-5894(84)90092-9)
- Midtbø I. 2011. A shoreline displacement curve for the Fosen area. In *Stone Age Settlements at the Fosen Peninsula, Stavanger, Skjelstad G* (ed). Museum of Archaeology, University of Stavanger: Stavanger; 61–64.
- Morén BM, Sejrup HP, Hjelstuen BO et al. 2018. The last deglaciation of the Norwegian Channel – geomorphology, stratigraphy and radiocarbon dating. *Boreas* **47**: 347–366. <https://doi.org/10.1111/bor.12272>
- Mur LR. 1969. The influence of brackish water on the growth of Chlorococcales particularly Scenedesmus. *SIL Proceedings, 1922–2010* **17**: 787–794. <https://doi.org/10.1080/03680770.1968.11895922>
- Nesje A. 1992. A piston corer for lacustrine and marine sediments. *Arctic and Alpine Research* **24**: 257–259. <https://doi.org/10.2307/1551667>
- Paus A. 1989. Late Weichselian vegetation, climate, and floral migration at Liastemmen, North Rogaland, south-western Norway. *Journal of Quaternary Science* **4**: 223–242. <https://doi.org/10.1002/jqs.3390040304>
- Paus A. 1990. Late Weichselian and Early Holocene vegetation, climate, and floral migration at Utsira, North-Rogaland, south-western Norway. *Norwegian Journal of Geology* **70**: 135–152.
- Peltier WR. 2004. Global glacial isostasy and the surface of the ice-age Earth: the ICE-5G (VM2) model and GRACE. *Annual Review of Earth and Planetary Sciences* **32**: 111–149. <https://doi.org/10.1146/annurev.earth.32.082503.144359>
- Pentecost A. 1984. *Introduction to Freshwater Algae*. Richmond Publishing.

- Ragnhildstveit J, Solli A. 1992. *Bedrock map of Skudeneshavn 1113 II, 1:50000*. Norwegian Geological Survey.
- Rao AR, Dayananda C, Sarada R et al. 2007. Effect of salinity on growth of green alga *Botryococcus braunii* and its constituents. *Bioresource Technology* **98**: 560–564. <https://doi.org/10.1016/j.biortech.2006.02.007>
- Reimer PJ, Bard E, Bayliss A et al. 2013. IntCal13 and Marine13 radiocarbon age calibration curves 0–50,000 years cal BP. *Radiocarbon* **55**: 1869–1887.
- Romundset A, Fredin O, Høgaas F. 2015. A Holocene sea-level curve and revised isobase map based on isolation basins from near the southern tip of Norway. *Boreas* **44**: 383–400. <https://doi.org/10.1111/bor.12105>
- Romundset A, Lakeman TR, Høgaas F. 2018. Quantifying variable rates of postglacial relative sea level fall from a cluster of 24 isolation basins in southern Norway. *Quaternary Science Reviews* **197**: 175–192. <https://doi.org/10.1016/j.quascirev.2018.07.041>
- Sejrup HP, Haflidason H, Aarseth I et al. 1994. Late Weichselian glaciation history of the northern North Sea. *Boreas* **23**: 1–13. <https://doi.org/10.1111/j.1502-3885.1994.tb00581.x>
- Sejrup HP, Nygård A, Hall AM et al. 2009. Middle and Late Weichselian (Devensian) glaciation history of south-western Norway, North Sea and eastern UK. *Quaternary Science Reviews* **28**: 370–380. <https://doi.org/10.1016/j.quascirev.2008.10.019>
- Shennan I, Bradley SL, Edwards R. 2018. Relative sea-level changes and crustal movements in Britain and Ireland since the Last Glacial Maximum. *Quaternary Science Reviews* **188**: 143–159. <https://doi.org/10.1016/j.quascirev.2018.03.031>
- Shennan I, Lambeck K, Horton B et al. 2000. Late Devensian and Holocene records of relative sea-level changes in northwest Scotland and their implications for glacio-hydro-isostatic modelling. *Quaternary Science Reviews* **19**: 1103–1135. [https://doi.org/10.1016/S0277-3791\(99\)00089-X](https://doi.org/10.1016/S0277-3791(99)00089-X)
- Shennan I, Rutherford MM, Innes JB et al. 1996. Late glacial sea level and ocean margin environmental changes interpreted from biostratigraphic and lithostratigraphic studies of isolation basins in northwest Scotland. *Geological Society, London, Special Publications* **111**: 229–244. <https://doi.org/10.1144/GSL.SP.1996.111.01.15>
- Stockmarr J. 1972. Tablets with spores used in absolute pollen analysis. *Pollen et Spores* **13**: 615–621.
- Stokes CR, Tarasov L, Blomdin R et al. 2015. On the reconstruction of palaeo-ice sheets: recent advances and future challenges. *Quaternary Science Reviews* **125**: 15–49. <https://doi.org/10.1016/j.quascirev.2015.07.016>
- Strunk A, Larsen NK, Nilsson A et al. 2018. Relative sea-level changes and ice sheet history in Finderup Land, North Greenland. *Frontiers in Earth Science* **6**: 129. <https://doi.org/10.3389/feart.2018.00129>
- Sundelin U. 1917. Fornsjöstudier inom Stångåns och Svartåns vattenområden: med särskild hänsyn till den sen-och postglaciala klimatutvecklingen. *Sveriges Geologiska Undersökning, Series CA* **16**: 291.
- Svendsen JI, Alexanderson H, Astakhov VI. 2004. Late Quaternary ice sheet history of northern Eurasia. *Quaternary Science Reviews* **23**: 1229–1271. <https://doi.org/10.1016/j.quascirev.2003.12.008>
- Svendsen JI, Briner JP, Mangerud J et al. 2015. Early break-up of the Norwegian Channel Ice Stream during the Last Glacial Maximum. *Quaternary Science Reviews* **107**: 231–242. <https://doi.org/10.1016/j.quascirev.2014.11.001>
- Svendsen JI, Mangerud J. 1987. Late Weichselian and Holocene sea-level history for a cross-section of western Norway. *Journal of Quaternary Science* **2**: 113–132. <https://doi.org/10.1002/jqs.3390020205>
- Tarasov L. 2013. GLAC-1b: a new data-constrained global deglacial ice sheet reconstruction from glaciological modelling and the challenge of missing ice. *Geophysical Research Abstracts* **15**, <https://meetingorganizer.copernicus.org/EGU2013/EGU2013-12342.pdf>.
- Vasskog K, Waldmann N, Bondevik S et al. 2013. Evidence for Storegga tsunami run-up at the head of Nordfjord, western Norway. *Journal of Quaternary Science* **28**: 391–402. <https://doi.org/10.1002/jqs.2633>
- vonAlvensleben N, Magnusson M, Heimann K. 2016. Salinity tolerance of four freshwater microalgal species and the effects of salinity and nutrient limitation on biochemical profiles. *Journal of Applied Phycology* **28**: 861–876. <https://doi.org/10.1007/s10811-015-0666-6>
- Wall D, Dale B, Harada K. 1973. Descriptions of new fossil dinoflagellates from the Late Quaternary of the Black Sea. *Micropaleontology* **19**: 18–31. <https://doi.org/10.2307/1484962>
- Ward SL, Neill SP, Scourse JD et al. 2016. Sensitivity of palaeotidal models of the northwest European shelf seas to glacial isostatic adjustment since the Last Glacial Maximum. *Quaternary Science Reviews* **151**: 198–211. <https://doi.org/10.1016/j.quascirev.2016.08.034>
- Yoshimura T, Okada S, Honda M. 2013. Culture of the hydrocarbon producing microalga *Botryococcus braunii* strain Showa: optimal CO₂, salinity, temperature, and irradiance conditions. *Bioresource Technology* **133**: 232–239. <https://doi.org/10.1016/j.biortech.2013.01.095>